Kinetic study of swelling-induced surface pattern formation and ordering in hydrogel films with depth-wise crosslinking gradient†

Murat Guvendiren,[a] Jason A. Burdick*[a] and Shu Yang*[b]

Received 4th January 2010, Accepted 17th February 2010
First published as an Advance Article on the web 22nd March 2010
DOI: 10.1039/b927374c

Hydrogels undergo extensive three-dimensional volume changes when immersed in water, the degree of which is determined by the network chemical composition and degree of crosslinking. When the hydrogel is attached to a rigid substrate, it swells preferentially perpendicular to the substrate. This anisotropic swelling generates a compressive stress, which drives the formation of surface patterns when exceeding a critical stress value ($\sigma \geq \sigma_c$). In order to develop an indepth understanding of the mechanism of surface pattern formation in hydrogels, we investigated the dynamic evolution of surface patterns in photocured hydrogel films from poly(2-hydroxyethyl methacrylate) (PHEMA) crosslinked with different concentrations of ethylene glycol dimethacrylate (EGDMA, 0–3 wt%). During curing in the presence of oxygen, a modulus gradient along the film depth was generated due to oxygen inhibition of the radical polymerization near the film surface. The swelling-induced wrinkling pattern formation followed Fickian-type kinetics ($\lambda \sim t^{1/2}$) at early stages, which was independent of the final pattern morphology. The onset of wrinkling was found at a linear expansion of $\alpha_c \approx 1.12$, which remained constant with increasing EGDMA concentration but decreased with increasing film thickness, indicating an increase in critical stress with crosslinker concentration. In contrast, the equilibrium linear expansion value, α_e, decreased significantly (from 2.55 to 1.20) with increasing crosslinker concentration (from 0 to 3 wt%), resulting in transition from random patterns to highly ordered hexagonal structures.

Introduction

Hydrogels are three-dimensional networks that can hold a large quantity of water. Because of the potential responsiveness to small environmental changes (*e.g.*, temperature, pH, and ion concentration), bicompatibility, and ability to store functional chemicals and nanoparticles, they have been investigated extensively for the past several decades.[1–3] Hydrogel thin films have been particularly intriguing lately as they can be used as tissue culture substrates,[4] sensors,[5] bioadhesives,[6] microfluidic devices[7] and responsive coatings.[8] In most of these applications, the hydrogel film is covalently attached to a much stiffer substrate, which restricts osmotic swelling at the film/substrate interface when the gels are exposed to a solvent. Thus, the film preferentially swells in the direction normal to the surface, affecting the structural and mechanical properties of the hydrogels, such as permeability and solvent-uptake.[9–13] Due to this anisotropic swelling, hydrogels experience an in-plane equibiaxial compressive stress, which is related to the equilibrium swelling of unconstrained hydrogel films in a stress-free state (Fig. 1a).[14–16] The degree of swelling and hence the magnitude of the compressive stress is dependent on the gel composition and extent of crosslinking. When the compressive stress exceeds a threshold value ($\sigma \geq \sigma_c$), an elastic surface instability arises to locally relieve the compressive stress, creating a variety of surface patterns (Fig. 1b).[13,17–20] When the compressive stress exceeds the elastic modulus and/or the interfacial adhesion strength between the gel and the substrate, the gel eventually delaminates.[21] Therefore, it is important to develop a greater understanding of the dynamics of swelling and surface instabilities to better control the pattern formation and surface properties of the surface-attached hydrogel films.[9,22]

Although much work has focused on manipulation of swelling-induced elastic instabilities in elastomeric films to form complex patterns,[23–27] there has been a renewed interest in controlling pattern formation and ordering in hydrogel films.[13,15,17,20,28] On a soft elastomer with a thin rigid skin, relatively small compressive stresses lead to formation of surface patterns,[29–34] and the mechanism can often be approximated by the classical plate theory.[31,32,35,36] For hydrogels, swelling induced instability arises due to constraint of the highly swollen film to a substrate, thus, leading to anisotropic osmotic pressure and relatively larger compressive stresses. Therefore, in addition to film modulus and strain level, crosslinking density and homogenity within the film, and film thickness could play important

[a]*Department of Bioengineering, University of Pennsylvania, 210 S 33th Street, Philadelphia, PA, 19104, USA. E-mail: burdick2@seas.upenn.edu; Fax: +1 (215) 573-2071; Tel: +1 (215) 898-8537*
[b]*Department of Materials Science and Engineering, University of Pennsylvania, 3231 Walnut Street, Philadelphia, PA, 19104, USA. E-mail: shuyang@seas.upenn.edu; Fax: +1 (215) 573-2128; Tel: +1 (215) 898-9645*

† Electronic supplementary information (ESI) available: Confocal fluorescent depth profiles of PHEMA gradient films, modulus and equilibrium water fraction of uniform PHEMA films, confocal microscopy images of PHEMA films swollen in water as a function of time, change of equilibrium film thickness, characteristic pattern size and amplitude *vs.* the initial film thickness, and change of critical expansion ratio with the initial film thickness. See DOI: 10.1039/b927374c

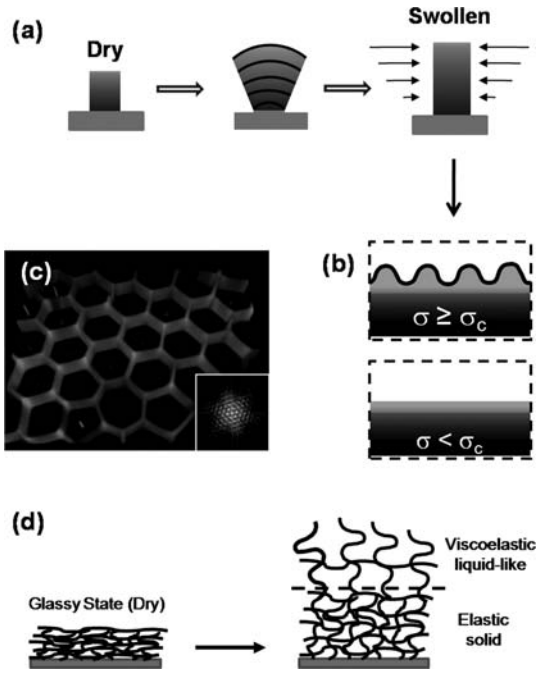

Fig. 1 **(a)** Illustration of swelling of a surface attached gel. The gel is under compressive stress due to anisotropic swelling perpendicular to the substrate. **(b)** When the stress is above the critical threshold, the gel surface buckles, or otherwise the surface remains flat. **(c)** 3D reconstruction of the optical image of PHEMA gel containing 3 wt% EGDMA after swelling and drying, showing the hexagonal pattern. Inset: FFT of the optical image. **(d)** An illustration of the PHEMA gel transition from dry (glassy) to the swollen (rubbery) state. Due to oxygen inhibition during photocrosslinking the outer surface of the water swollen gel behaves like a viscoelastic liquid whereas the bulk remains elastic. The illustration is not to scale.

roles in controlling pattern morphology and characteristic size.[13,15,17]

Recently, we have reported the formation of a wide range of surface patterns in swollen poly(2-hydroxyethyl methacrylate) (PHEMA) hydrogel films confined onto a flat substrate, from random worm-like structures in transit to peanut shape, lamellar and a highly ordered hexagonal pattern.[20] The key difference in our approach compared to prior reports on swelling-induced patterns on hydrogels is that we create a depth-wise modulus gradient by manipulating O_2 diffusion during the UV curing process. In addition, because of the glassy nature of the dried PHEMA, the de-swelling kinetics is not the same as for swelling. Instead, the surface patterns formed during swelling are kinetically trapped during drying, leading to stable patterns in both wet and dry states (Fig. 1c). The observed hydrogel surface patterns in the present work are in the form of shallow undulations, "wrinkles", which is fundamentally different than the "creasing" patterns in the form of localized sharp folds reported in highly-swollen polyacrylamide hydrogels[13,15] The "creasing" patterns can be obtained in our gradient hydrogels by increasing the solvent quality, and thus swelling ratio. A detailed comparison between crease and wrinkle formation will be reported elsewhere. We note that all of the observations and characterizations of pattern formations are based on the equilibrium states, where the gels are swollen for a long period of time, followed by drying in air.

Here, we present a detailed kinetics study of gradient PHEMA gels, including their initiation and growth as a function of time in comparison with the equilibrium states in order to develop a better understanding of the mechanisms of pattern formation and transition between different pattern orders. The changes in pattern size (λ) and amplitude (A), and film thickness (h) of the hydrogel films were monitored *in situ* by confocal microscopy during swelling in water. We observed a Fickian-type pattern growth behavior, $\lambda \sim t^{1/2}$, which was independent of pattern morphology. Our results suggest that we can tune the equilibrium linear expansion with the crosslinker concentration, and thus the pattern morphology. The critical linear expansion, on the other hand, is slightly decreased with increasing crosslinker concentration and initial film thickness. Furthermore, we find that when the linear expansion value approaches the critical linear expansion, patterns with perfectly hexagonal order are initiated; however, the degree of equilibrium linear expansion determines whether the hexagonal order remains stable or not when the gel continues to swell and reaches equilibrium.

Results and discussion

PHEMA films with depth-wise crosslinking gradients were prepared by photopolymerization of the precursor solution in the presence of oxygen (*i.e.*, open to air). During radical photopolymerization, dissolved oxygen acted as a radical scavenger, which lowered the crosslinking density of the hydrogels, and the concentration of oxygen in the film was determined by the oxygen diffusion profile from the top surface into the film (Fig. 1b, and Fig. S1†). Details of fabrication and characterization of these gradient PHEMA films can be found in our earlier study.[20]

Initially, the crosslinked gradient-PHEMA films were in solvent-free glassy states and covalently attached to the rigid glass substrates. When exposed to water, water diffused into the film at the surface. However, the confinement of the film to the rigid substrate restricted osmotic swelling in the direction parallel to the substrate (xy plane), creating an equibiaxial compressive stress (Fig. 1a), the degree of which was determined by the network composition and extent of crosslinking. Swelling of a constrained gel can be considered as uniaxial expansion, where the linear extension ratio (α) is equal to the volumetric degree of swelling (V):

$$\alpha = \frac{h}{h_0};\ V = \frac{\phi_0}{\phi} \tag{1}$$

$$\frac{h}{h_0} = \frac{1}{\phi} \tag{2}$$

Here, h and h_0 are the swollen and dry film thicknesses, respectively, and ϕ and ϕ_0 (= 1) are the polymer fractions of the swollen and dry films, respectively. For PHEMA hydrogel films, the equilibrium water fraction ($\phi_w = 1 - \phi_e$) was determined by the crosslinker (EGDMA) concentration (Fig. 2). For uniformly crosslinked films (polymerized with a cover),[20] the highest swelling, $\phi_w = 0.13 \pm 0.02$, was obtained for films without EGDMA. ϕ_w then dropped sharply to ~0.09 with 0.5 wt%

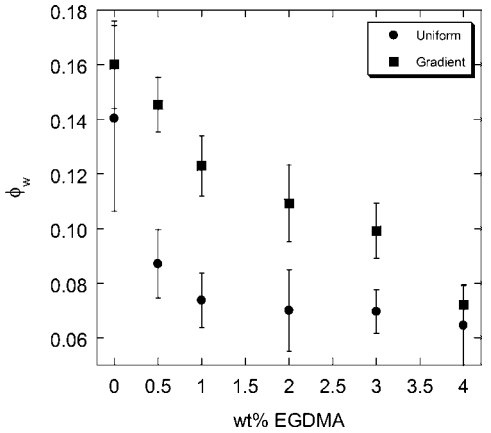

Fig. 2 Equilibrium water fraction (ϕ_w) of uniform and gradient PHEMA hydrogel films *vs.* EGDMA concentration.

EGDMA, and gradually afterwards with increasing EGDMA concentration. The opposite trend was observed for Young's modulus (see Fig. S2†). For uniform gels, only random swelling patterns were formed without EGDMA. However, for gradient films, ϕ_w values were higher when compared with uniform films with the same EGDMA loadings. For example, $\phi_w = 0.16$ and 0.10 in gradient films compared to 0.14 and 0.07 in uniform films with 0 and 3 wt% EGDMA, respectively. For gradient films, patterns were observed for all formulations with $\leq$4 wt% EGDMA, at which point swelling approached that of the uniform film. These results suggest that the outer surface of the gradient film is much softer than the uniform gels, much like a viscoelastic liquid (see Fig. 1d), thus, creating a much larger compressive stress to generate surface wrinkling patterns.

In order to understand pattern formation dynamics, we studied the time-dependent evolution of characteristic wavelength of the surface patterns, $\lambda(t)$. Sequences of images captured by optical microscopy during water swelling of a PHEMA film ($\sim$60 μm thick) with 2 wt% EGDMA are shown in Fig. 3a. When the crosslinked dry film was exposed to water, surface instability was initiated and the pattern began growing within 60 s (Fig. 3b). Pattern formation started with a finer hexagonal pattern, which remained stable, but the pattern size increased gradually and reached an equilibrium value, λ_{eq}. The pattern size and morphology were maintained after the gel was dried (Fig. 3b). Further study showed that λ_{eq} decreased with increasing EGDMA concentration, whereas it increased with increasing initial film thickness (Fig. 4). For hydrogel thin films, we assume that $\lambda(t)$ is proportional to the deformation along the z axis (normal to the substrate), $u(z,t)$, since this diffusion length is the only relevant length scale.[19] This behavior can be explained by linear diffusion, or Fickian-type kinetics, where $\partial u/\partial t = D\partial^2 u/\partial z^2$, and the solution of $u(t)/u(\infty) \approx \lambda(t)/\lambda(\infty)$ is[37,38]

$$\lambda(t) = \lambda_{eq}\left(1 - (8/\pi)\sum_{n=0}^{\infty}(2n+1)^{-2}\, e^{(-t/\tau_n)}\right) \qquad (3)$$

where $\lambda(\infty)$ is denoted by λ_{eq}, $\tau_n = \tau/(2n+1)^2$, and $\tau = (\alpha_e h_0)^2/[(\pi/2)^2 D]$, and α_e is the equilibrium linear expansion and D is the effective diffusion coefficient. Eqn (3) can be further simplified for a short (eqn (4)) and a long period of swelling time (eqn (5)), respectively:[38]

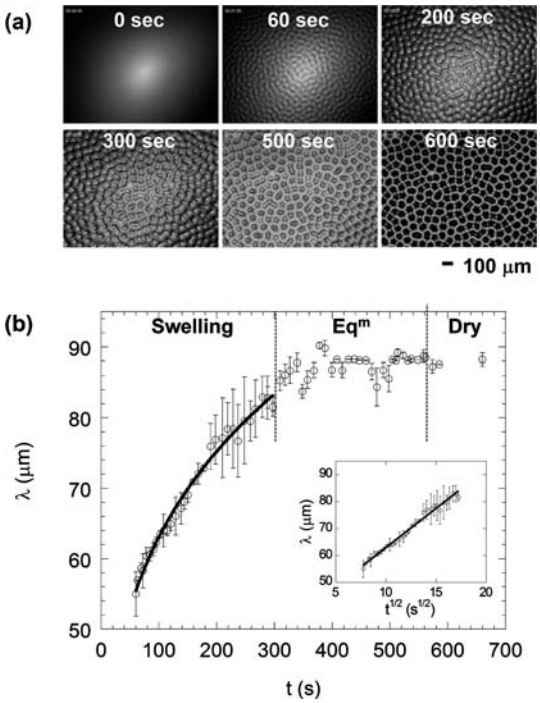

Fig. 3 **(a)** Snapshots of optical images showing the evolution of hexagonal patterns formed on a PHEMA hydrogel film with 2 wt% EGDMA (dry thickness $\sim$60 μm) when swollen in DI water. **(b)** Characteristic pattern size (λ) plotted against elapsed time. Dotted lines separate the swelling region, gel in equilibrium, and dry gel. Inset: λ *vs.* $t^{1/2}$.

$$\lambda(t) = (1 - 1/\alpha)(Dt)^{1/2} \qquad (4)$$

$$\lambda(t) = \lambda_{eq}(1 - (8/\pi^2)e^{(-t/\tau)}) \qquad (5)$$

Although this methodology assumes one-dimensional (1D) uniform diffusion, while in practice the diffusion is nonlinear due to the depth-wise crosslinking gradient in our PHEMA gels, we found that the initial growth of λ did follow a $t^{1/2}$ relationship (see Fig. 3b inset) as shown in eqn (4). The pattern growth rate decreased for a longer swelling time, relaxing to a final equilibrium state, which was well fitted by eqn (5). D values were calculated from Fig. 4a in the range of 1.96×10^{-7} cm^2 s^{-1} (3 wt% EGDMA) up to 4.60×10^{-7} cm^2 s^{-1} (0 wt% EGDMA). These values were an order of magnitude smaller than the D value ($\sim 5 \times 10^{-6}$ cm^2 s^{-1}) for surface-attached acrylamide gels obtained from the morphological change of surface patterns (similar to our analogy).[38] Therefore, pattern formation kinetics were much slower in our PHEMA gel system when compared with acrylamide hydrogels, enabling us to directly visulize pattern initiation and growth in a greater detail. We observed that the initial order of the patterns was hexagonal (Fig. 5), independent of EGDMA concentration. Individual hexagons nucleated from different locations on the gel surface, rapidly consuming the undeformed (flat) regions. Transient defects (dislocations) were observed when the boundary of these deformed regions came into contact. The orientation mismatch between neighboring hexagons mostly disappeared with time for PHEMA films with 2 wt% and 3 wt% EGDMA.

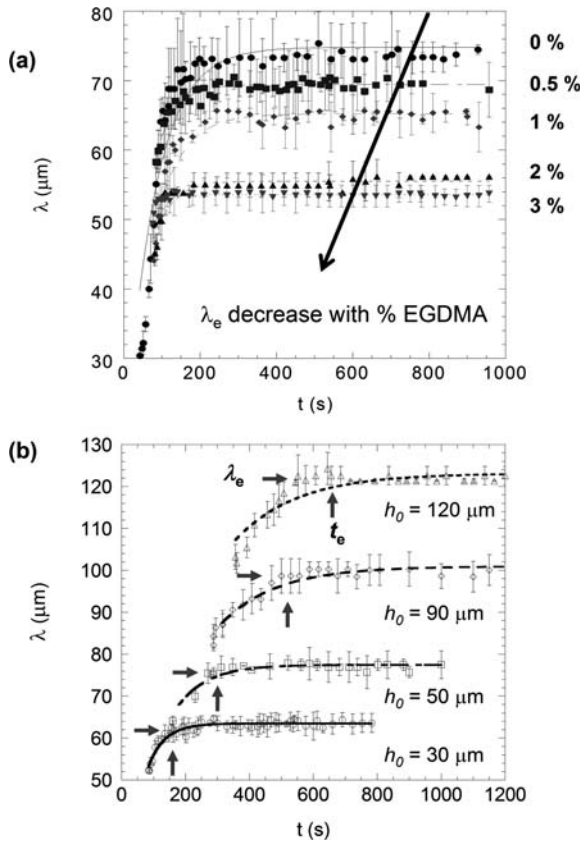

Fig. 4 Time evolution of characteristic wavelengths of patterns (λ) of PHEMA hydrogels during swelling in water. **(a)** The effect of crosslinker (EGDMA) concentration (for $h_0 = 30$ μm). **(b)** The effect of initial film thickness (h) (for 1 wt% EGDMA). The equilibrium wavelength (λ_e, indicated by the plateau value) significantly decreased with EGDMA concentration and decreasing film thickness. Lines represent the fits using eqn (4) and (5) for short and long swelling time, respectively.

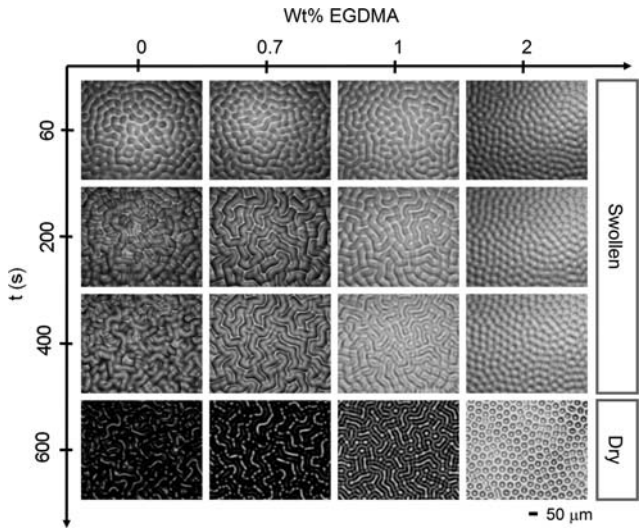

Fig. 5 Optical microscope images showing the evolution of swelling patterns for PHEMA hydrogels with and without EGDMA. The dry film thickness was ~30 μm. In each system, swelling patterns originated from a hexagonal order and evolved to reach its equilibrium state with time, which was determined by the EGDMA concentration.

The initially formed finer hexagonal pattern continued to grow with time and collapsed into peanut (1 wt% EGDMA), worm-like (0.5 wt% EGDMA) and irregular (0 wt% EGDMA) morphologies depending on the crosslinker concentration (*i.e.* the gradient) (Fig. 5). In comparison, the initial hexagonal order remained for films with 2 and 3 wt% EGDMA, whereas no patterns were formed with EGDMA ≥4 wt%. We believe that our observations are consistent with previous pattern ordering theory for swelling hydrogels.[13,38] Specifically, Tanaka *et al.* have suggested that when the osmotic stress is equal to the critical value a hexagonal order is obtained, which becomes distorted when the stress exceeds this threshold ($\sigma \geq \sigma_c$).[13] As $\sigma = E\,\varepsilon(\alpha,\phi)$, where E is modulus and strain ε is a function of either the linear expansion ratio (α) or polymer fraction (ϕ) in the swollen gel, there must be a window within close proximity to the critical linear expansion value (α_c) in which the hexagonal patterns are stable for EGDMA concentrations between 2 and 3 wt%. When EGDMA concentration is decreased, $\alpha > \alpha_c$ and the hexagonal order becomes distorted. Thus, the degree of distortion, and hence the equilibrium morphology, can be controlled by the relative linear expansion, or the crosslinker concentration.

The real time change in total swollen film thickness (h_s), pattern amplitude (A) and λ during water swelling was monitored *via* confocal microscopy. We used xy-scans (parallel to the surface) to obtain λ and pattern order, and xz-scans (depth profiles) to measure A and h_s. The confocal snapshots (at t = 15 min) of xy- and xz-scans are given for 3 wt% EGDMA in Fig. 6a and 6b, respectively. A red fluorescent dye (PolyFluor™ 570) was added to the precursor solution prior to UV exposure for confocal imaging of the gels. A typical plot of the data obtained from confocal microscopy is provided in Fig. 6c, which

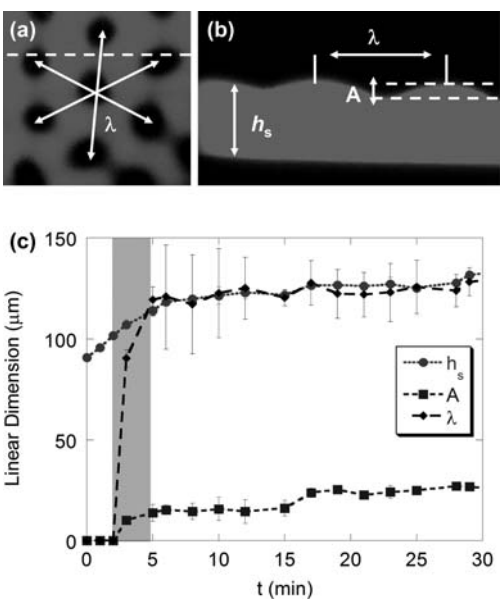

Fig. 6 Confocal microscopy images of PHEMA hydrogel films (3 wt% EGDMA) in DI water. **(a)** xy-scan (surface profile) and **(b)** xz-scan (depth profile) at t = 13 min. **(c)** Change of characteristic pattern size (λ), total swollen film thickness (h_s), and pattern amplitude (A) with time (t). Cross-linked gel (dry at $t = 0$) was placed in a chamber filled with DI water. The data was obtained from the images of same location of the gel. The shaded area represents the pattern evolution regime where λ and A increases.

shows the change in λ, A, and h_s with elapsed time. The first data point in the plot (at $t = 0$ min) was from a crosslinked gel in a solvent-free state. After this initial scan, the sample chamber was filled with water and the film swelled as water diffused from the top surface. The height of the gel increased almost instantaneously, whereas an induction period was necessary for the pattern to develop, during which h_s increased gradually (see Fig. S3†). For instance, for 3 wt% EGDMA, h_s increased from 85 μm to 100 μm in order for patterns to initiate. The shaded area in Fig. 6c indicates the pattern growth region, where λ and A increased sharply before reaching equilibrium. As seen in Fig. S4,† the corresponding equilibrium values, h_{eq}, λ_{eq} and A_{eq}, decreased with EGDMA concentration, and increased with the initial film thickness.

A was calculated for each time point (Fig. 7a) according to eqn (1). As long as the film surface remained flat, the swollen thickness of the film was equal to the total film thickness h_s. When patterns appeared on the film surface, the swollen thickness (h_t) was measured from the half maximum of the pattern amplitude, assuming constant volume (Fig. 7b). α_c for pattern formation was then determined from the onset of change in λ and A (starting point of shaded area in Fig. 7a). α_c remained constant with increasing EGDMA concentration but decreased slightly with increasing initial film thickness (see Fig. S5†). The equilibrium linear expansion ratio (α_e) was plotted against crosslinker concentration in Fig. 8. For each EGDMA concentration, α_e was the average value measured for films with thickness in the range of 90–300 μm. α_e decreased significantly with increasing EGDMA concentration. For PHEMA films without EGDMA, $\alpha_e = 2.54 \pm 0.53$, for 0.5 wt% EGDMA, $\alpha_e = 2.39 \pm 0.36$, which significantly decreased to 1.37 ± 0.11 for 1 wt% EGDMA. For 3 wt% EGDMA, $\alpha_e = 1.19 \pm 0.36$, which was very close to the critical value. The solid line in Fig. 8 denotes α_c values (1.14 ± 0.10), below which the swollen film surface remainded flat. α_e decreased significantly with increasing EGDMA concentration.

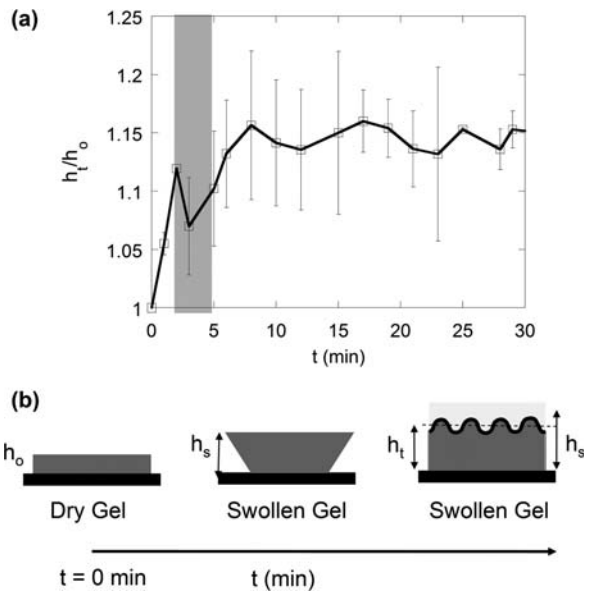

Fig. 7 **(a)** The change in extension ratio of the PHEMA hydrogel (3 wt% EGDMA) during swelling. **(b)** As the water diffuses into the network, the gel can only expand in the direction perpendicular to the substrate due to constraint to substrate. h_0 is the initial (dry) thickness, h_t is the time dependent swollen gel thickness, and $h_t = h_s - (A/2)$, where A is the amplitude after patterns formed. h_s is the total swollen film thickness.

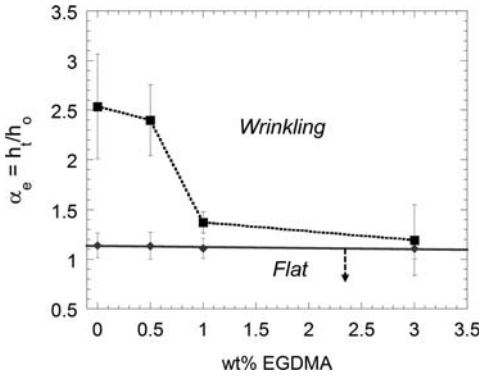

Fig. 8 The change in the equilibrium expansion ratio (α_e) for PHEMA films with EGDMA concentration. The solid line in the figure represents the critical values, α_c, below which the hydrogel surface remains flat.

Conclusions

We investigated the dynamic evolution of osmotically driven surface patterns in PHEMA hydrogels with depth-wise crosslinking gradients. It was observed that pattern evolution followed the Fickian-type kinetics, $\lambda \sim t^{1/2}$ relationship, at early swelling stages, regardless of the final pattern morphology and size. The equilibrium pattern size and elapsed time to equilibrium were determined by the initial film thickness and EGDMA concentration. Our results showed that the critical linear expansion (α_c) remained constant with increasing EGDMA concentration but decreased slightly with increase of the initial film thickness (h_0). This finding is important because the stress magnitude in the hydrogel depends on the crosslink density and the constant critical linear expansion indicates the critical stress should vary with EGDMA concentration. Therefore, our results invalidate the critical stress criteria proposed in the previous studies.[14–16] We showed that highly ordered and stable hexagonal patterns were formed when the equilibrium linear expansion (α_e) was just above α_c when EGDMA concentration was between 2 and 3 wt%. However, when $\alpha_e \gg \alpha_c$, the hexagonal order was transient and could be distorted. The final pattern morphology was then determined by α_e, which could be fine-tuned by crosslinker concentration. For these PHEMA hydrogels, hexagons coalesced into peanuts for 1 wt% EGDMA, lamellar patterns for 0.5 wt% EGDMA, and complete random structures for PHEMA without crosslinker. We believe that the presented study of swelling kinetics of the PHEMA gels with gradient crosslinking density will shed light on how to control long-range ordering in swelling-induced pattern formation, for example, using non-homogeneous gels.

Experimental

PHEMA prepolymer was prepared by UV exposure (UVP Black Ray, 8 mW cm^{-2}) of 2-hydroxyethyl methacrylate (HEMA, 2 mL, 98%, Alfa Aesar) as monomer and the Darocur 1173 (3 wt%, 60 μL, Ciba Specialty Chemicals) as photoinitiator for 60 s. Another mixture of Darocur 1173 and the crosslinker, ethylene glycol dimethacrylate (EGDMA, Polysciences) (2 : 1 wt

ratio), was added to the viscous prepolymer to form the PHEMA precursor solution. A series of precursor solutions without and containing EGDMA (0.5 wt% to 3 wt%) were prepared (stable for several months when kept in the dark).

PHEMA films were fabricated using a Micrometer Adjustable Film Applicator (S271727, Sheen Instruments Ltd., Kingston, England). Micrometer heads were set to the desired precursor film thickness and a glass slide was placed under the blade and the heads were calibrated. The precursor was added in front of the blade and the applicator was gently drawn along the glass slide. Precursor coated glass slides were then exposed to UV light (Omnicure S1000 UV Spot Cure System, Exfo Life Sciences Division, Mississauga, Ontario, Canada) for 20 min (10 mW cm^{-2}, 365 nm) either covered ('uniform') or uncovered ('gradient'). In order to covalently attach the film to the substrate during UV exposure, glass slides were functionalized with 3-(trimethoxysilyl)propyl methacrylate (TMS, Aldrich) by covering the surface of the glass slides ($1'' \times 1''$ coverslip) with TMS (100 μL) immediately after UV-ozone treatment (Jelight UVO, Model 144AX) for 30 min, followed by two step annealing (100 °C for 30 min, then 110 °C for 10 min). Glass slides were then rinsed thoroughly in DI water and dried overnight.

Optical microscopy was performed on an Olympus BX61 motorized microscope with Hamamatsu controller. For kinetic studies, images were captured automaticaly (1 image per 3 s). Confocal microscopy imaging was performed on a Nikon TE300 inverted microscope fitted with a Bio-Rad Radiance 2000 MP3 system (Bio-Rad Laboratories, Inc., Hercules, CA). Images were observed through a 10× and/or 20× objective, and recorded with Lasersharp 2000 software (Bio-Rad Laboratories, Inc.). A fluorescent dye, methacryloxyethyl thiocarbonyl rhodamine B (PolyFluor™ 570, Polysciences, Warrington, PA), was added to the precursor to obtain contrast (gel appeared red under fluorescent light). Depth profiles were obtained by collecting xz-scans with 1 μm step size. For kinetic studies, 2 scans per minute were performed. All measurements were completed in ImageJ (1.41n, National Institute of Health).

Acknowledgements

The research is funded in part by National Science Foundation MRSEC DMR05-20020, an NSF CAREER award DMR-0548070 (SY), and a Fellowship in Science and Engineering from the David and Lucile Packard Foundation (JAB).

Notes and references

1 Z. H. Nie and E. Kumacheva, *Nat. Mater.*, 2008, **7**, 277–290.
2 N. A. Peppas, J. Z. Hilt, A. Khademhosseini and R. Langer, *Adv. Mater.*, 2006, **18**, 1345–1360.
3 A. Sidorenko, T. Krupenkin, A. Taylor, P. Fratzl and J. Aizenberg, *Science*, 2007, **315**, 487–490.
4 N. Mari-Buye, S. O'Shaughnessy, C. Colominas, C. E. Semino, K. K. Gleason and S. Borros, *Adv. Funct. Mater.*, 2009, **19**, 1276–1286.
5 I. Tokarev and S. Minko, *Soft Matter*, 2009, **5**, 511–524.
6 M. Guvendiren, D. A. Brass, P. B. Messersmith and K. R. Shull, *J. Adhes.*, 2009, **85**, 631–645.
7 S. R. Quake and A. Scherer, *Science*, 2000, **290**, 1536–1540.
8 V. Kozlovskaya, E. Kharlampieva, I. Erel and S. A. Sukhishvili, *Soft Matter*, 2009, **5**, 4077–4087.
9 R. Toomey, D. Freidank and J. Ruhe, *Macromolecules*, 2004, **37**, 882–887.
10 M. E. Harmon, D. Kucking and C. W. Frank, *Langmuir*, 2003, **19**, 10660–10665.
11 M. E. Harmon, D. Kuckling and C. W. Frank, *Macromolecules*, 2003, **36**, 162–172.
12 M. E. Harmon, D. Kuckling, P. Pareek and C. W. Frank, *Langmuir*, 2003, **19**, 10947–10956.
13 T. Tanaka, S. T. Sun, Y. Hirokawa, S. Katayama, J. Kucera, Y. Hirose and T. Amiya, *Nature*, 1987, **325**, 796–798.
14 S. K. Basu, A. V. McCormick and L. E. Scriven, *Langmuir*, 2006, **22**, 5916–5924.
15 V. Trujillo, J. Kim and R. C. Hayward, *Soft Matter*, 2008, **4**, 564–569.
16 S. K. Basu, L. E. Scriven, L. F. Francis and A. V. McCormick, *Prog. Org. Coat.*, 2005, **53**, 1–16.
17 J. S. Sharp and R. A. L. Jones, *Phys. Rev. E: Stat., Nonlinear, Soft Matter Phys.*, 2002, **66**, 011801.
18 K. Sekimoto and K. Kawasaki, *J. Phys. Soc. Jpn.*, 1987, **56**, 2997–3000.
19 T. Hwa and M. Kardar, *Phys. Rev. Lett.*, 1988, **61**, 106–109.
20 M. Guvendiren, S. Yang and J. A. Burdick, *Adv. Funct. Mater.*, 2009, **19**, 3038–3045.
21 J. Y. Chung, K. H. Kim, M. K. Chaudhury, J. Sarkar and A. Sharma, *Eur. Phys. J. E*, 2006, **20**, 47–53.
22 M. Gianneli, R. F. Roskamp, U. Jonas, B. Loppinet, G. Fytas and W. Knoll, *Soft Matter*, 2008, **4**, 1443–1447.
23 D. P. Holmes and A. J. Crosby, *Adv. Mater.*, 2007, **19**, 3589–3593.
24 D. P. Holmes, M. Ursiny and A. J. Crosby, *Soft Matter*, 2008, **4**, 82–85.
25 Y. Zhang, E. A. Matsumoto, A. Peter, P. C. Lin, R. D. Kamien and S. Yang, *Nano Lett.*, 2008, **8**, 1192–1196.
26 D. Breid and A. J. Crosby, *Soft Matter*, 2009, **5**, 425–431.
27 J. Y. Chung, A. J. Nolte and C. M. Stafford, *Adv. Mater.*, 2009, **21**, 1358–1362.
28 Y. Klein, E. Efrati and E. Sharon, *Science*, 2007, **315**, 1116–1120.
29 E. Cerda and L. Mahadevan, *Phys. Rev. Lett.*, 2003, **90**, 074302.
30 X. Chen and J. W. Hutchinson, *J. Appl. Mech.-Trans. ASME*, 2004, **71**, 597–603.
31 J. Groenewold, *Phys. A*, 2001, **298**, 32–45.
32 R. Huang, *J. Mech. Phys. Solids*, 2005, **53**, 63–89.
33 W. T. S. Huck, N. Bowden, P. Onck, T. Pardoen, J. W. Hutchinson and G. M. Whitesides, *Langmuir*, 2000, **16**, 3497–3501.
34 E. Sultan and A. Boudaoud, *J. Appl. Mech.-Trans. ASME*, 2008, **75**, 051002.
35 N. Bowden, S. Brittain, A. G. Evans, J. W. Hutchinson and G. M. Whitesides, *Nature*, 1998, **393**, 146–149.
36 K. Efimenko, M. Rackaitis, E. Manias, A. Vaziri, L. Mahadevan and J. Genzer, *Nat. Mater.*, 2005, **4**, 293–297.
37 A. Onuki, *J. Phys. Soc. Jpn.*, 1988, **57**, 703–706.
38 H. Tanaka, H. Tomita, A. Takasu, T. Hayashi and T. Nishi, *Phys. Rev. Lett.*, 1992, **68**, 2794–2797.